Biosensors and Bioelectronics 207 (2022) 114206

Contents lists available at ScienceDirect

Biosensors and Bioelectronics

journal homepage: www.elsevier.com/locate/bios

Reversible photonic hydrogel sensors via holographic interference lithography

Samuel Davies [a], Yubing Hu [a,*], Nan Jiang [b,**], Yunuen Montelongo [c], Andreas Richardson [a], Jeff Blyth [a], Ali K. Yetisen [a]

[a] Department of Chemical Engineering, Imperial College London, London, SW7 2BU, UK
[b] West China School of Basic Medical Sciences & Forensic Medicine, Sichuan University, Chengdu, 610041, China
[c] Department of Engineering Science, University of Oxford, Oxford, OX1 3PJ, UK

ARTICLE INFO

Keywords:
Photopolymerization
Optical pH sensors
Holography
Hydrogels
Biosensor

ABSTRACT

Continuous monitoring of physiological conditions and biomarkers *via* optical holographic sensors is an area of growing interest to facilitate the expansion of personalised medicine. Here, a facile laser-induced dual polymerization method is developed to fabricate holographic hydrogel sensors for the continuous and reversible colorimetric determination of pH variations over a physiological range in serum (pH 7–9). Readout parameters simulated through a Finite-difference time-domain Yee's algorithm retrieve the spectral response through expansion. Laser lithography of holographic hydrogel sensor fabrication is achieved *via* a single 355 nm laser pulse to initiate polymerization of ultrafine hydrogel fringes. Eliminating the requirement for complex processing of toxic components and streamlining the synthetic procedure provides a simpler route to mass production. Optimised pH-responsive hydrogels contain amine bearing functional co-monomers demonstrating reversible Bragg wavelength shifts of 172 nm across the entire visible wavelength range with pH variation from 7.0 to 9.0 upon illumination with broadband light. Photolithographic recording of information shows the ability to convey detailed information to users for qualitative identification of pH. Holographic sensor reversibility over 20 cycles showed minimal variation in replay wavelength supporting reliable and consistent readout, with optimised sensors showing rapid response times of <5 min. The developed sensors demonstrate the application to continuous monitoring in biological fluids, withstanding interference from electrolytes, saccharides, and proteins colorimetrically identifying bovine serum pH over a physiological range. The holographic sensors benefit point-of-care pH analysis of biological analytes which could be applied to the identification of blood gas disorders and wound regeneration monitoring through colorimetric readouts.

1. Introduction

Analysis of pH is important to a wide range of fields linked to modern life, including agriculture (Smith and Doran, 1997), environmental monitoring (Doney et al., 2009), pharmaceutical manufacture (Alibrandi et al., 2001) and biomedical applications (Zulkarnay et al., 2015). With the growing movement towards personalised medicine, the demand for point-of-care (POC) diagnostic devices is of paramount importance (Yetisen et al., 2013; Yager et al., 2008; Luppa et al., 2011). Medical professionals have expressed the consistent desire for POC devices to assist in the diagnosis, management, and treatment of acute or chronic illnesses (Howick et al., 2014). Factors such as cost or lack of specificity and reliability hinder the adoption of optical technologies (Shaw, 2016), advances in biosensor technology has had to ensure devices that are accessible *via* the development of low-cost, accurate, and user-friendly diagnostic systems (Zarei, 2017; Dincer et al., 2017). In this regard, optical sensors demonstrate their advantages of superior stability, selectivity, and simplicity of readout. Holographic sensors function in the visible wavelength region to be interpreted qualitatively by the naked eye without the requirement for specialised equipment (Hu et al., 2014; Jiang et al., 2018). This simplistic readout has been previously utilised to achieve both qualitative and quantitative measurements to specific analytes, such as organic solvent (Yetisen et al., 2014a), alcohols (Jiang et al., 2021), ions (Mayes et al., 2002), glucose

* Corresponding author.
** Corresponding author.
E-mail addresses: yubing.hu@imperial.ac.uk (Y. Hu), jiangnansophia@scu.edu.cn (N. Jiang).

https://doi.org/10.1016/j.bios.2022.114206
Received 25 November 2021; Received in revised form 8 March 2022; Accepted 19 March 2022
Available online 21 March 2022

(Kabilan et al., 2005a), and ionic strength(Marshall et al., 2004). Holographic sensors can display colorimetric response through chemically stimulated volumetric changes to a hydrogel with nanostructured variation in refractive index (RI) (Tjandra et al., 2020b). Quantitative measurements *via* a spectrophotometer analysis through widely available technology such as smartphone cameras permits expansion of POC devices (Kim et al., 2019). At present, POC monitoring utilises electrical, colorimetric, and fluorescent sensors. Electrical sensors are often susceptible to signal drift over time and are incompatible with several modern medical techniques such as magnetic resonance imaging (Koch et al., 2010). Conventional electrochemical sensors are bound by the requirement for an electrical power source to initiate sensing; however holographic sensors are power-free and label-free devices, expanding potential applications (Davies et al., 2021). Colorimetric and fluorescent sensors are the most widely utilised optical POC devices such as lateral flow assays (Sajid et al., 2015; Weidgans et al., 2004). Despite their fast and sensitive response, fluorescent sensors are often susceptible to photobleaching, signal interference from concentration variation, and environmental change (Song et al., 1995; Altschuh et al., 2006). Unlike fluorescent sensors, holographic sensors allow for reversible and continuous monitoring of homeostasis without the risk of photobleaching. Therefore, the development of holographic optical biosensors will assist in the evolution of medical care.

Holographic sensors rely upon RI variation which can be achieved through a range of techniques such as photolithographic recording of nanocomposites (Leite et al., 2010), and inorganic nanoparticles (NP) (Yetisen et al., 2014b). With the most prominent technique in literature being *in-situ* photo-reduction of metal ions such as silver to form NP fringe structures (i.e. AgNP) (Kawata et al., 2009). Metal NPs deliver the change in RI required for holographic sensors, but improvements are required for mass production and application to biological sensing. The complex chemistry used in the reduction and fixing of metal NPs mandates a high number of processing steps, which has been a major hindrance to mass production and widespread application. The removal of the requirement for NP components can be achieved *via* the use of secondary hydrogel polymerization to reduce the requirement for inorganic species. Utilising the dual photo-polymerized systems, the number of steps is reduced significantly improving the opportunity to move towards widespread use. Moreover, there is a hesitation within regulatory bodies about the *in vivo* application of metal NPs, linked to a lack of information of their metabolism within the body and possible linkage to carcinogenic behaviour, impeding their approval in medical devices. The absence of metal NPs in the dual photo-polymerized holographic structures decreases the possible risks in biomedical monitoring (Kawata et al., 2009; Asare et al., 2012).

pH is one of the most important physiological conditions monitored in healthcare. Nearly all biological processes are affected by pH variations such as enzyme conformation (Chattopadhyay and Mazumdar, 2000), ion transport (Skou, 1998), and cell membrane tension (Petelska and Figaszewski, 2000). Wound pH can be correlated with angiogenesis, protease activity and bacterial infection (Percival et al., 2014; DPhil et al., 2005). Healthy skin pH varies from 4.0 to 6.0, upon injury pH rises to a more neutral pH (7.4), due to exposure to the biological material beneath (Jones et al., 2015a). Variation can differ depending upon wound severity with chronic injuries previously recorded at neutral to alkaline (7.2–8.9) values (Gethin, 2007). Healing occurs more readily in an acidic environment. However, alkaline or extremely acidic pH values can indicate a bacterial infection (Jones et al., 2015b). Monitoring pH in wound tissue may provide an analytical platform, ultimately enabling determination of response to treatment. Alternatively, pH sensing can be applied to arterial blood pH analysis in the diagnosis of blood gas disorders such as acidosis or alkalosis. With a healthy blood pH between 7.35 and 7.45, variations outside of this range can be correlated to imbalances in dissolved gases, possible indication of uncontrolled diabetes, haemorrhage, and pulmonary failure. Conventional blood sampling often incurs patient discomfort, reducing adherence to the testing regime and ultimately inducing a lack of patient devotion to medical regimes that reduces data reliability (Colletti et al., 1995). Biocompatible polymers, such as 2-hydroxyethyl methacrylate (HEMA), can be used in the fabrication of optical hydrogels sensors and can be located *in-situ* for continuous measurement. Therefore, facilitating earlier diagnosis, and treatment of disease due to ease of use and reversible readout. Consequently, there is a currently unmet requirement for biocompatible continuous and reversible optical pH monitoring to improve the management of many ailments.

Here, a single-flash ultraviolet dual photo-polymerized method is developed to produce holographic sensors for reversible and continuous analysis of physiological pH. Computational modelling of volumetric changes effect on replay wavelength accelerates the optimisation process of the sensors. Simulations allow for projections regarding sensor performance with greater simplicity and promptness than physical experimentation. The reliability of these predictions depends on the strength of agreement between the computational model and the experimental results, as well as the applicability and assumptions of parameters used throughout the modelling process. The synthesis utilised a single pulse from a Nd:YAG laser system ($\lambda_m = 355$ nm) to initiate dual photo-polymerization of highly cross-linked fringes within a loosely cross-linked pH responsive hydrogel matrix to produce holographic sensors. Demonstrating rapid monitoring of pH over a physiological range with simple optical readouts capable of being determined both qualitatively through visual inspection and quantitatively through a spectrophotometer analysis. The research presented details the functionalised dual photo-polymerized system with the effect of comonomers concentration, crosslinking density, and thickness variation. Properties of the holographic hydrogel pH sensors such as angular dependency, diffraction efficiency and reliability of wavelength are also described. The developed sensors show high selectivity to pH independent from common biological contaminates, minimal replay wavelength variation over 20 cycles, and sensitivity of 0.0068 pH nm^{-1} with optimised sensors showing response times of 5 min.

2. Results and discussion

2.1. Computational modelling of holographic sensor fabrication and readout

The critical function in the sensor operation is the interaction of light with the holographic sensor. The relationship has been described by Braggs law (Eqn. (1)) (Kang et al., 2007).

$$n\lambda_{max} = 2d \sin\theta \quad (1)$$

where λ_{max} is the reflected wavelength (nm), d is the interfringe spacing, and θ is the angle of illumination from the normal. The peak replay wavelength (λ_{max}) is dependent upon the spacing (d) of the fringes recorded within the matrix. Sensitisation is achieved *via* the use of smart hydrogels which gratings are recorded within. Upon introduction of a stimulus, the hydrogel volume increases or decreases varying d, and therefore the replay wavelength. Here, an implementation of the Finite-difference time-domain (FDTD) Yee's algorithm in Matlab (software) is proposed (Yetisen et al., 2014c). Fig. 1a illustrates the recording process of the holographic sensor simulation to correlate with the experimental fabrication method. Effective RI of the recording hydrogel is set to that of water at 1.34, due to the high moisture content of the hydrogel. Simulated laser exposure is emitted as a planar wave form from the left side of the simulation propagating through the recording material, and then reflecting from a mirrored surface (Fig. 1a–i). All areas excluding the recording matrix and glass had a RI set to 1. Interference between the incident and reflected waves produce an interference pattern of nodes and antinodes within the recording matrix. Fig. 1 a-ii highlights the exposure energy profile of the counter propagating beams. Antinodes recorded within the matrix had RI set to 1.64, comparable to

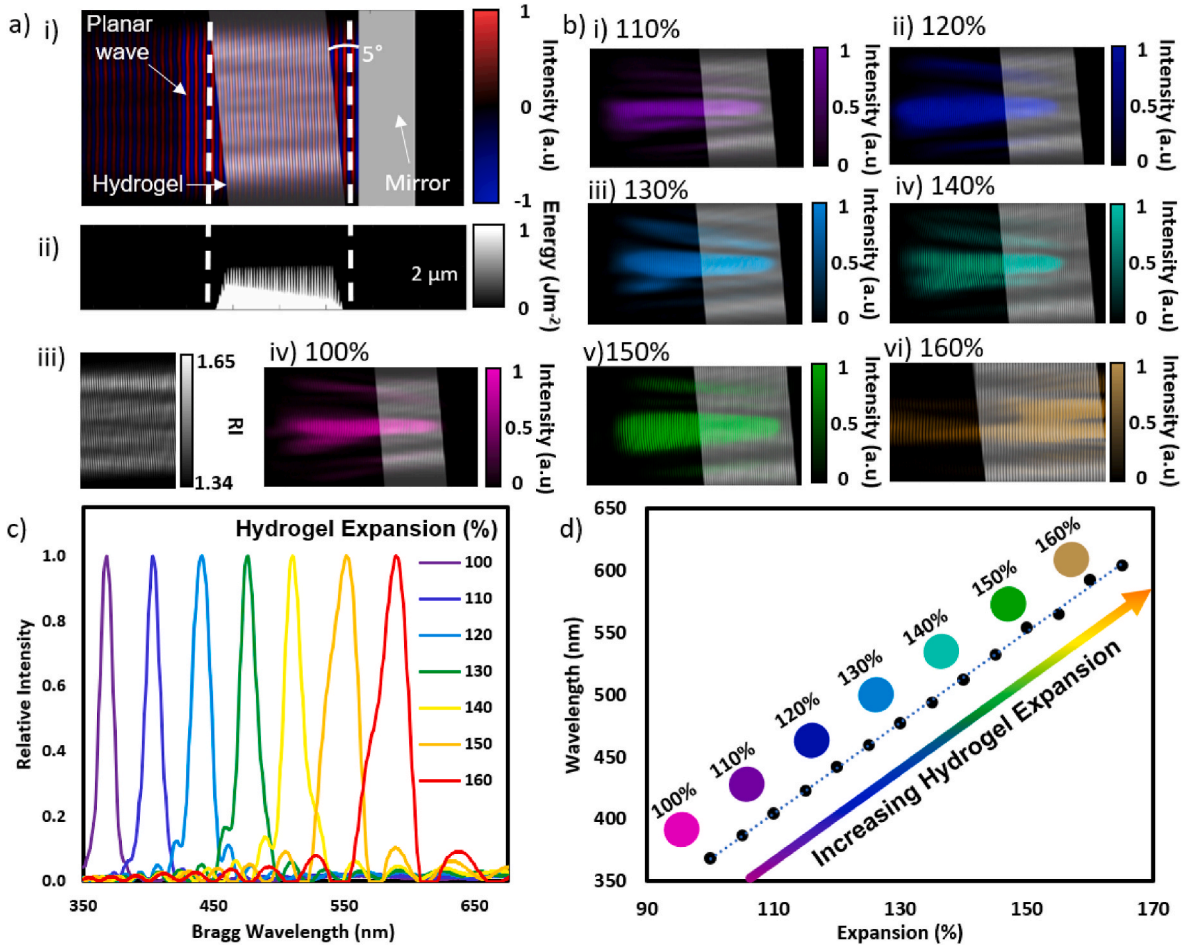

Fig. 1. Simulation of holographic sensor recording and readout. a) i) Screenshot of wave propagation throughout hydrogel matrix during the recording process with a 355 nm beam, ii) total exposure energy throughout the hydrogel upon wave propagation, iii) structure of holographic sensor depicted through the variation of RI through the hydrogel, iv) diffraction of incident light at 100% hydrogel expansion. b) Simulation of diffracted of light through grating at different hydrogel expansions from 110% to 160%. c) Simulated Bragg peak spectrum for hydrogel expansion values of 100–160% after repeating multiple reading simulations. d) Peak shift in the wavelength diffracted observed during expansion, inset depicts colors expected for individual expansion values.

experimental RI monomer mixtures at a ratio of 1:2 (v/v) (pH responsive matrix: interference layer) (Fig. 1a–iii). The reading output clearly demonstrated a wavelength of ideal intensity for the specific fringe spacing; to adequately measure the wavelength of greatest interaction spectra of individual wavelengths were recorded as they propagate through the hydrogel with the reflection intensity monitored. Fig. 1b shows the reflection simulation results with the corresponding wavelength for the grating at expansions of 100%, 110%, 120%, 130%, 140%, 150%, and 160% giving spectral responses of 368, 404, 442, 477, 512, 554, and 592 nm respectively (Movie S1). Simulated Bragg reflection peaks are highlighted in Fig. 1c. To further demonstrate this linear relationship trend observed in the diffraction peak, diffractions were monitored over the whole range at intervals of 5% with the spectral peaks and simulated colors obtained was displayed in Fig. 1d. Considering the 223 nm peak shift observed for 60% expansion in simulation, an approximate hydrogel expansion of 3.73% per nm was calculated. This simulation provides a first approximation to the complex relationship between optical response and hydrogel swelling.

Supplementary data related to this article can be found at https://doi.org/10.1016/j.bios.2022.114206.

2.2. Fabrication of holographic hydrogel pH sensor

The holographic sensors are composed of two alternating hydrogel layers of differing RI. A low RI pH responsive matrix which consists of a low crosslinking density hydrogel, into this a second-high RI interference layer containing high crosslinking density is polymerized by laser photo-lithography. This *in-situ* polymerization generates alternating layers of low and high RI hydrogels to form a holographic Bragg structure. These structures can tune the reflection of a narrow band of wavelengths which can be correlated with chemically stimulated expansion of the hydrogel. Concentrations of monomers are varied throughout to further examine their effect on the sensor response, the pH responsive matrix was prepared by a free radical polymerization of a hydrophilic monomer (Hydroxyethylmethacrylate, HEMA, >61 mol%), and a functional *co*-monomer (Dimethylaminoethyl acrylate, DMAEA, 5–25 mol%) and crosslinker (Ethylene glycol dimethylacrylate, EGDMA, 2–6 mol%) initiated by a photoinitiator (2-Hydroxy-2-methyl-propiophenone, HMPP, 1 mol%) (Fig. 2a–i). The interference layer is composed of highly crosslinked polymer network utilising HEMA (13 mol%), EGDMA (84 mol%) and HMPP (3 mol%) (Fig. 2a–ii). The low crosslinking density in the pH responsive matrix of the hydrogel allows for large volume variations depending upon the protonation and deprotonation of the co-monomer. The smart hydrogel employed in the responsive matrix contains functional *co*-monomer, DMAEA, which bears a tertiary amine, is capable of being protonated and deprotonated at different pH values (Marshall et al., 2003). The level of protonation is dependent on the acidic association constant (pK_a) of the amines lone pair of electrons and their ability to donate electron density to protons within solution (Ofridam et al., 2021). DMAEA has been identified as an

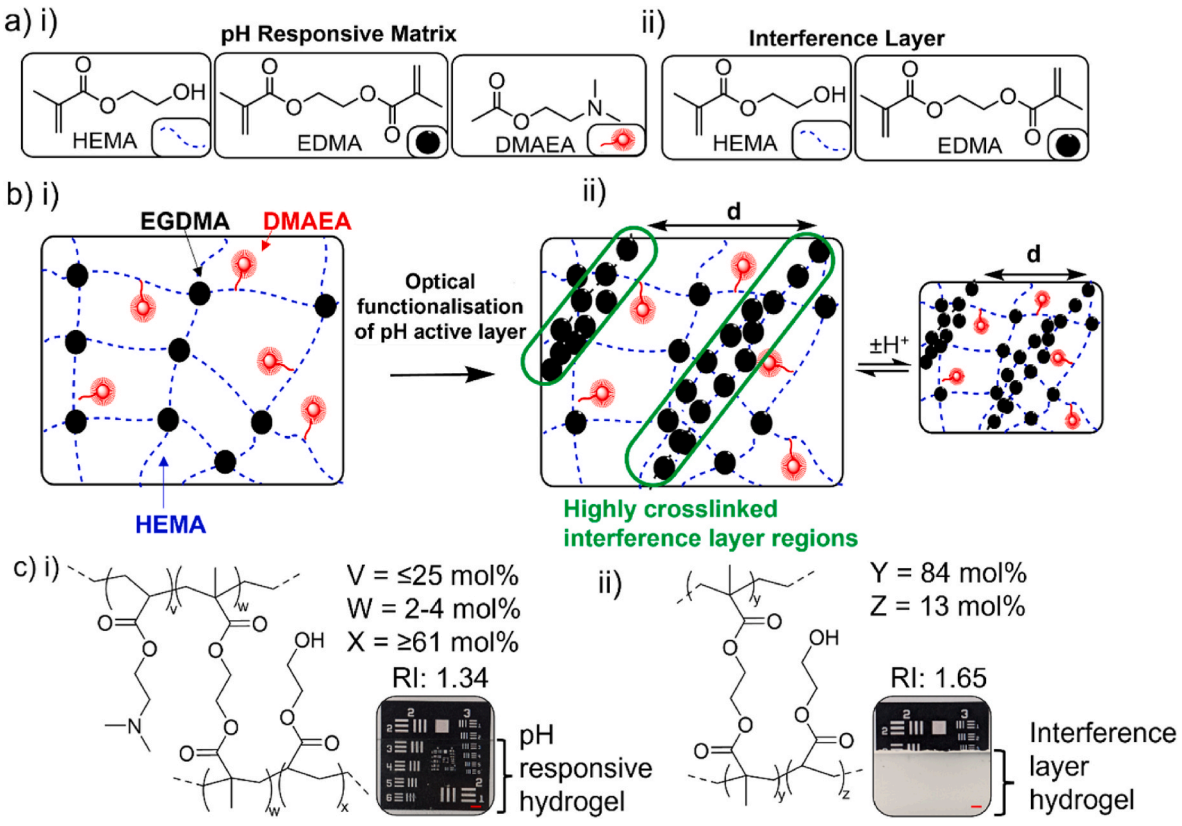

Fig. 2. Chemical structures and fundamentals of the holographic hydrogel pH sensor. a) Chemical structures of i) pH responsive matrix monomers and ii) Interference layer monomers inset images demonstrate the two hydrogels post-polymerization, insets show photographs of the polymerized monomer solutions; b) Schematic to display hologram construction i) with and ii) without interference layers recorded, where d illustrates the spacing between the interference layer fringes; c) The respective polymeric networks of the i) responsive matrix and ii) interference layer alongside photographs of the two hydrogels separately polymerized on transparent glass slides covering the bottom half of the USAF resolution target (scale bar = 2 mm).

ideal candidate for hydrogel functionalisation, due to the slightly basic pK_a, providing a sensitivity range encompassing the normal physiological ranges of biological fluids, i.e. blood (7.35–7.45) and cerebrospinal fluid (CSF) (7.33–7.52). Although DMAEA was selected due to the pK_a, a variety of *co*-monomers such as methacrylic acid or 2-Acrylamido-2-methylpropane sulfonic acid could be applicable to tune the sensitivity range of the sensor to alternate pH ranges. The responsive hydrogel utilises a relatively low crosslinker concentration (2–6 mol%), whereas the interference layer contains 84 mol% of crosslinker. Disparity in crosslinking density generates the change in RI, when swollen required to produce a Bragg nanostructure (Fig. S1) (Askadskii, 1990). The interference layer differs by the concentration of crosslinking, with the pH-responsive layer and interference layer containing <6 mol% and 84 mol% of EGDMA respectively, restricting swelling and increasing RI producing the holographic nanostructure (Fig. 2b–c). The visual difference between the two hydrogels can be observed in Fig. 2c, where the highly crosslinked hydrogel shows an opaque white color, while the responsive matrix with low crosslinking shows transparency. Effective RIs of the two distinct hydrogels were determined to be 1.34 and 1.65 for the pH responsive matrix and interference layer, respectively.

A schematic overview of the fabrication process and mechanism of optical sensing is illustrated in Fig. 3a. Through the optimisation of hydrogel composition, the dual photopolymerised fabrication method is utilised to generate a response over the whole visible spectrum. Monomer solutions throughout this process were freshly prepared for each experiment and aerated prior to each experiment, as it is hypothesized dissolved oxygen in monomer solutions inhibits radical migration in the recording process which can affect grating consistency (Hageman, 1985). There are 4 main steps to the fabrication process: responsive matrix polymerization, incorporation of interference layer monomers, recording of the holographic sensor followed by the development of the grating (Fig. 3a). Firstly, the responsive hydrogel is polymerized onto a glass slide which has been silanized with 3-tri(methoxy silyl)propyl methacrylate (Fig. 3a–i). This was done so that a methacrylate group can be covalently bonded to the glass surface *via* Si–O bonds, then photo-polymerized with the pH-responsive hydrogel, this is imperative for the effective attachment of the hydrogel to the glass slide. Polymerized hydrogels were washed in a hot methanol bath (50 vol%, 60 °C) and the secondary monomer solution for the interference layer was subsequently applied (Fig. 3a–ii). Samples were left to soak for 10 min before drying under a cool air flow. As the recording wavelength is in the UV region, shrinkage of the hydrogel post recording led to a replay wavelength in the deep UV, outside the visible region. Therefore, by recording the hydrogel in a dry state, submerging into an aqueous analyte solution post exposure leads to hydrogel swelling, bringing the replay wavelength into the visible region.

The holographic structures fabricated depend upon the use of a coherent frequency tripled Nd:YAG laser source (5 ns, 355 nm, 40 μs delay) to initiate polymerization of alternating multilayers of hydrogels at regular spacings within a pH-responsive hydrogel. A single flash was utilised to generate polymerization, by utilising a single flash, the risk of multiple recording points is minimised due to lack of any nano-movements. Holographic sensors were recorded in reflection mode where the interference pattern between the incident beam and the reflected object beam form nodes and anti-nodes, areas of high and low intensity UV light, fringe spacings of gratings were determined by the wavelength of incident light (Fig. 3b) (Kreis, 2004). Anti-nodes, areas of constructive interference, decompose HMPP to initiate free radical photo-polymerization of the interference layer within the pH-responsive hydrogel. In contrast nodes, areas of destructive interference, lack

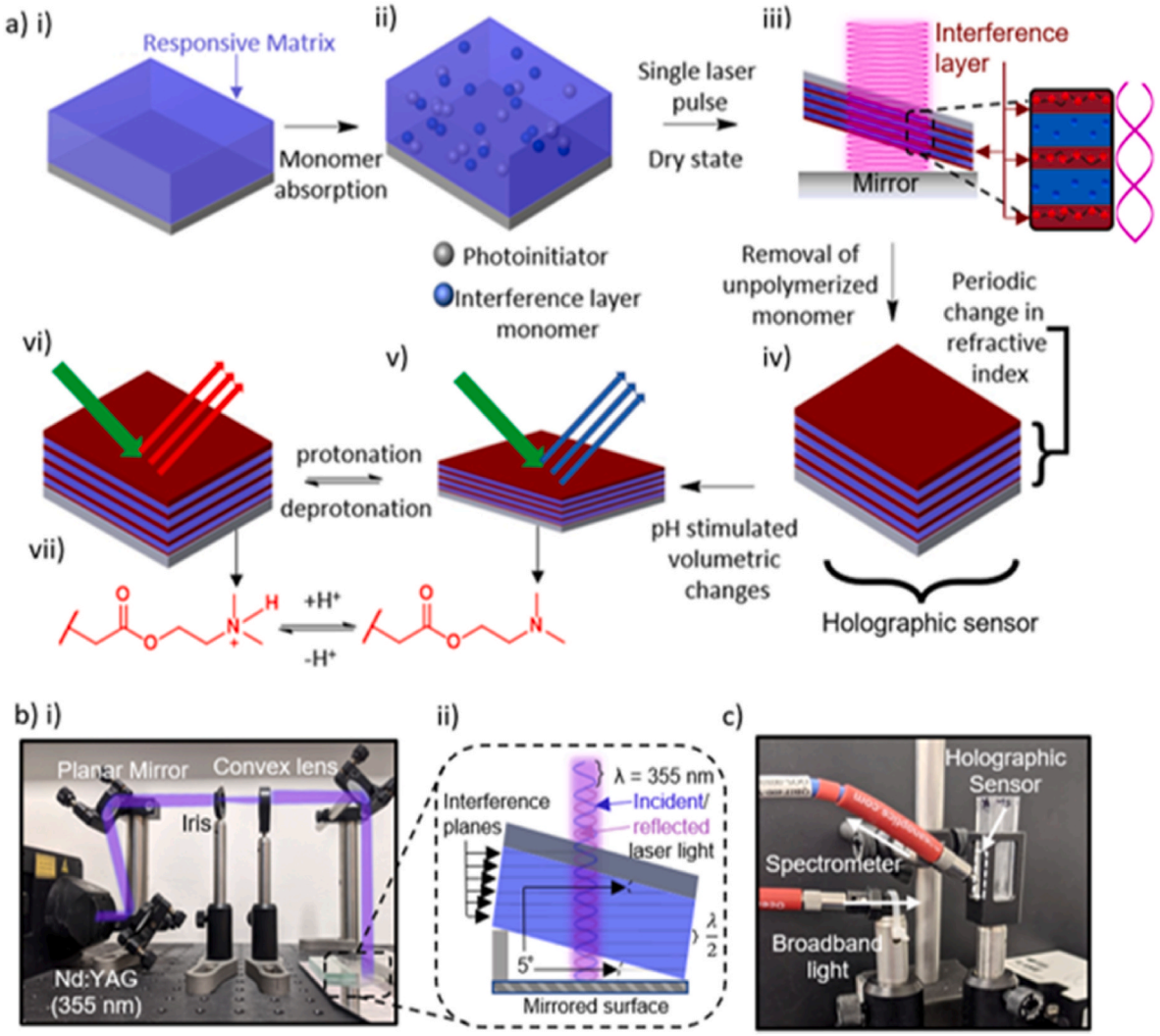

Fig. 3. Fabrication and interrogation processes of dual photo-polymerized holographic pH sensors. i) Hydrogels containing functional co-monomer DMAEA, ii) diffusion of monomers into functionalised hydrogel matrix, iii) exposure of photosensitised hydrogel at a 5° angle to a single UV pulse laser (355 nm), iv) removal of unpolymerized monomers, v) blue shifting of replay wavelength at high pH, vi) red shifting of replay wavelength at low pH, vii) equilibrium process that incurs the swelling/shrinking behaviour of the hydrogel pH sensor. b) Photograph and schematic to demonstrate the fabrication process of the pH sensitive optically active hydrogel. i) Photograph to illustrate the optical set up utilised to fabricate the holographic hydrogels, ii) detailed illustration of the interference pattern from the incident laser light to generate the alternating points of polymerization within the hydrogel sensor. c) Grating interrogation set up including a broadband light source and a spectrophotometer.

photo-polymerization (Fig. 3a iii-iv) with unpolymerized monomers removed *via* subsequent washing steps in a fresh MeOH:H_2O bath (1:1, v/v). Protonation of DMAEA, produced an ionic charge within the hydrogel network, changing the hydration level of the hydrogel due to changes in osmotic and electrostatic forces from the movement of counter ions across the layers of hydrogel (Fig. 3a v-vii) (De et al., 2002). These changes in solvation alter the swelling/shrinkage of the hydrogel; and therefore the spacing of the interference layers, tuning the replay wavelength. Fig. 3b illustrates the exposure set up utilised to induce the counter propagation of incident and reflected beams to create the interference pattern required for reflection holography (Fig. 3b–ii). Fig. 3c highlights the readout set up, where the tuned reflected wavelength is separated from the specular reflection due to the 5° recording angle. Sensors show a high degree of reproducibility in the fabrication process, within this research sensors have been refabricated several times whilst maintaining comparable replay wavelength ranges. Fig. S2 highlights the replay wavelengths of 3 separately prepared holographic sensors at pH 7, where an average replay wavelength of 631 nm with an error margin of 3.2 nm.

2.3. Characterisation of holographic hydrogel pH sensors

To investigate the effect of the thickness on the diffraction efficiency of the holographic sensors and the rate of wavelength variation, the volume of monomer solution for the pH-responsive matrix was varied. The thicknesses of the hydrogel sensor with 25 μm (T1), 28 μm (T2), 30 μm (T3), 35 μm (T4), and 38 μm (T5) were prepared with monomer volumes at 25 μL, 37.5 μL, 50 μL, 62.5 μL, and 75 μL respectively (Fig. 4c i-v). The hydrogel sensors were dehydrated under vacuum for 24 h, to ensure minimal residual hydration and consistent swelling across all samples. To determine the optimum thickness of the hydrogels, two characteristics were monitored, namely brightness of the hologram and rate of peak equilibration in TRIS buffer at pH 7 (50 mmol L^{-1}). The relative intensity of the reflection rises until a plateau for thicknesses above 30 μm, showing relative intensities of 0.32 (T1), 0.55 (T2), 0.93 (T3), 0.92 (T4) and 0.95 (T5) (Fig. 4a). The slight red shift of replay wavelength observed in T4 sits within the error margin expected for these sensors. It is hypothesized to be linked to the decreased the number of layers recorded within the responsive matrix in thinner

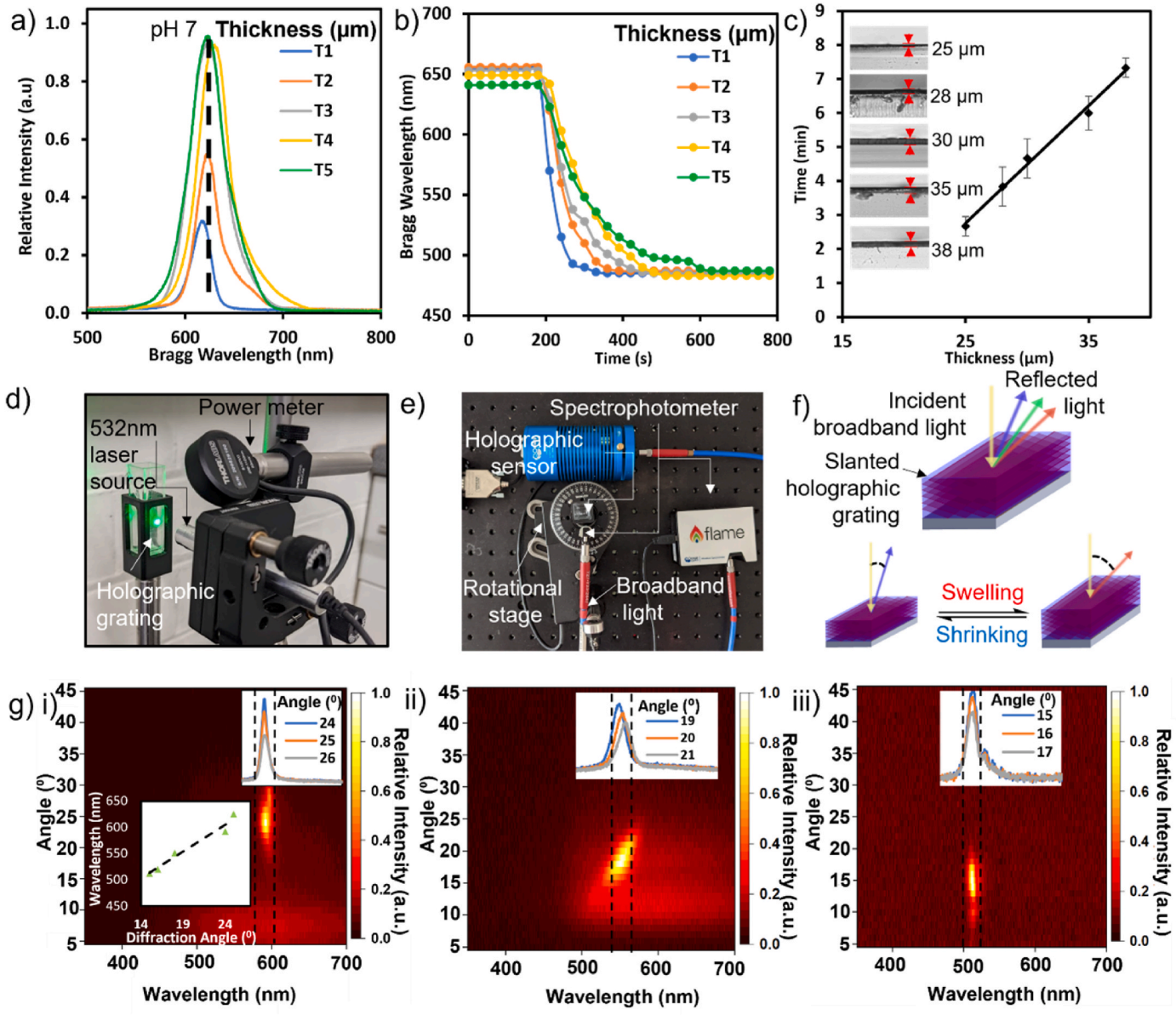

Fig. 4. Thickness and angular replay dependency of the holographic sensor; a) Bragg replay wavelength as a function of thickness in tris-buffer solution (pH 7, 50 mmol L^{-1}, KCl). b) Rate of movement for the sensors with differing thickness. c) A graph to demonstrate the relationship between hydrogel thickness and response time, microscope images of holographic hydrogels with thicknesses 25 μm, 28 μm, 30 μm, 35 μm, and 38 μm, where error bars represent the calculated standard error of 3 independent sets of results. d) Diffraction efficiency measurement set up with 532 nm laser and power meter. e) Optical set up utilised to record the angle of highest intensity reflection. f) Relationship of diffraction angle to reflection wavelength recorded from holographic sensors. g) Angular measurements from rotational stage for holographic sensors with replay wavelengths of i) 592 nm, ii) 550 nm, and iii) 520 nm, inset highlights the diffraction at angles of greatest intensity.

hydrogels, resulting in reduced diffraction efficiency. Equilibration time was monitored of all hydrogel sensors to determine the optimised thickness. This was achieved by timing the interval for Bragg replay wavelength to stabilise when shifting from pH 7–9. Replay wavelengths were monitored at intervals (30 s) until peak stabilisation was achieved. Determined rates for each thickness were 2.5 min (T1), 3.5 min (T2), 5 min (T3), 5.5 min (T4), and 7 min (T5) (Fig. 4b–c). It can be concluded that the thickness of the hydrogel sensor is directly related to the rate of movement of the peak. T3 was selected to be ideal, as the intensity of the peak was on the same order of brightness as that of thicker hydrogels with an acceptable response time. Thus, a volume of 50 μL was identified as the optimised monomer volume for the polymerization of the responsive hydrogel matrix. With all sensors of varying thickness showing comparable wavelength shift, the degree of relative expansion is expected to be analogous. For the 5 different dry thicknesses produced experimentally (Fig. 4c, inset), the expansion percentage can be inferred *via* computational simulations, results indicated that an expansion of 50% is required to cover the visible regime (Fig. S3). For optimised film thickness 30 μm a 50% expansion range of 33 μm–48 μm can be inferred throughout measurements." Diffraction efficiency was determined *via* illumination with a 532 nm laser, with the respective diffractions monitored by using a power meter (Fig. 4d). By utilising a rotational stage for the receiving spectrophotometer, the angular dependency of the reflection was established (Fig. 4e). As previously described in the fabrication, the hologram is recorded with an elevation of 5° to ensure reflected light is easily distinguishable from specular reflection. Slanted holographic sensors therefore demonstrate an angular variation directly linked the volumetric swelling of the hydrogel (Fig. 4f). The dependency on swelling is directly related to Bragg's law, where spacing (d) and wavelength (λ) are related to the angle (θ) (Eqn. (1)). The diffraction

angle varies minimally between the swollen and unswollen state. The angle of highest intensity decreases upon shrinking of the hydrogel (swollen = 25°, unswollen = 15° (Fig. 4g, Fig. S4)). The variation of angle can lead to a requirement for the repositioning of the spectrophotometer receiving cable which should be considered when monitoring hologram readout. Minimum sample volume was determined to be 100 μL, through the utilisation of a horizontal optical set up (Fig. S5a). Droplets of buffer solutions at pH 7 and 9 were alternately placed onto an illuminated section of holographic grating and the optical response observed (Fig. S5b). Sensors showed no clear error in sensitivity and maintained a total shift of 179.5 nm over three cycles. At values lower than 100 μL effective coverage of the holographic sensor was not reliably achievable.

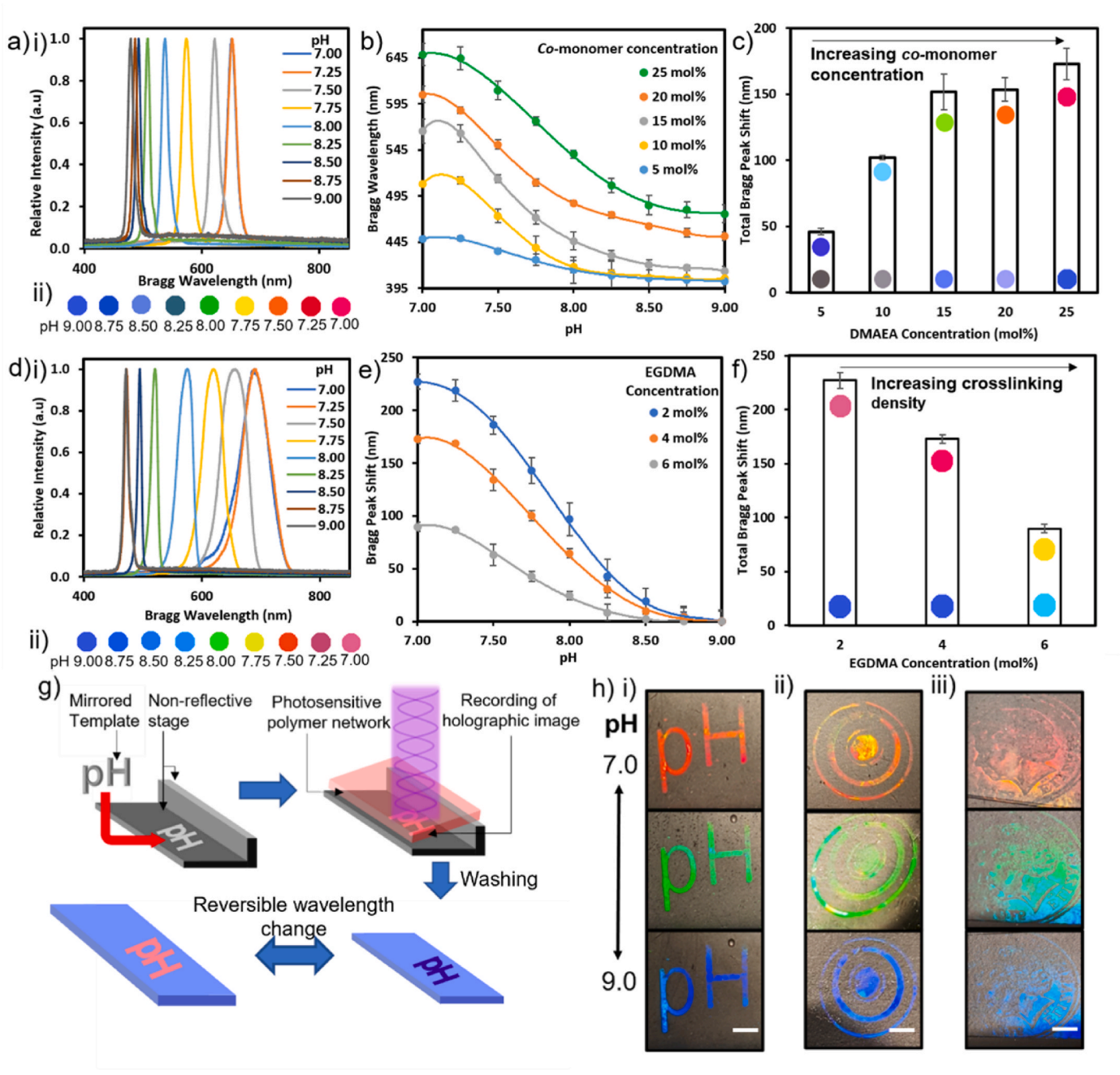

Fig. 5. Effect of the monomer concentration on the hydrogel sensing. a) i) Normalised Bragg reflection wavelength from gratings containing 25 mol% of DMAEA over a pH range of 7–9, ii) cropped smartphone images of colorimetric sensor response. b) Bragg wavelength change observed for hydrogel sensors containing functional DMAEA concentrations of 5–25 mol%, where error bars represent the calculated standard error of 3 independent sets of results. c) Total change in Bragg peak that occurs with the change of pH from 7 to 9 along with the color changes observed, where error bars represent the calculated standard error of 3 independent sets of results. d) Normalised Bragg reflection peaks of a grating containing EGDMA (2 mol%) from pH 7–9, ii) cropped smartphone captured images of colorimetric sensor response. e) Plot of the relative Bragg reflection peak change for crosslinking monomer concentrations (2–6 mol%), where error bars represent the calculated standard error of 3 independent sets of results. f) the total shift observed for each grating and its corresponding cropped smartphone image of the color change, where error bars represent the calculated standard error of 3 independent sets of results. g) Schematic illustrating the recording process of artistic holograms. h) Observable colour change of holographic sensor when changing from pH 7–9 recorded with i) 'pH' character, ii) concentric circle pattern, and iii) a coin to illustrate sensing properties (scale bar = 4 mm), images for each sensor were collected with a smartphone positioned at 20° relative to the hologram surface.

2.4. DMAEA concentration variation

Sensitisation of developed hydrogels to pH was achieved *via* the incorporation of co-monomer DMAEA. Fig. 5a demonstrates the change in Bragg peak wavelength with increasing DMAEA concentration over a physiological pH range (7–9). The concentration of the functional co-monomer impacted the swelling generated *via* changes in the electrostatic and osmotic forces with variation of bound ionic charge in the hydrogels (Fig. 5a–c, Fig. S6). Increased DMAEA concentration expanded shifting range, comparing 5 mol% vs 25 mol%, with Bragg peak shift ranges of 45.8 nm and 172.7 nm, respectively. An effective pK_a of the gratings was calculated to be 7.89, in contrast to the unpolymerized pK_a of DMAEA of 8.3, a variation of −0.41 pK_a units (Cotanda et al., 2013). Various factors determine the pK_a of the polyelectrolyte, such as the hydrophobicity of the environment and the level of hydrogen bonding within the structure (Tang et al., 2018; Li et al., 2016). Dual photo-polymerized holograms when compared to the AgNP systems previously demonstrated offer a slightly lower range of shifting, due to increase crosslinking density (Marshall et al., 2003). High crosslinking density within interference layers effectively increases crosslinking density throughout the hydrogel, diminishing the ability to obtain large peak shifts with low concentrations of co-monomers (2–8 mol%). Therefore, DMAEA concentration was increased to improve the spectral range. Fig. 5b–c demonstrates the replay wavelengths and total shift range of the varied DMAEA formulations. Formulations from 5 mol% to 15 mol% show a linear relationship where total shift increases with increasing DMAEA concentration. DMAEA concentrations above 15 mol % produce a plateau in total shift, the wavelength range varied. The maximum replay wavelength ranges of 15 mol% DMAEA is from 565 nm (pH 7) to 413 nm (pH 9), whereas 25 mol% of DMAEA shows a range from 648 nm (pH 7) to 475 nm (pH 9). Increasing the baseline shift improves contrast between the colors observed, i.e., 15 mol% colour range is blue to green, whereas 25 mol% shifts from blue to red. Colorimetric changes are discernible through the naked eye, allowing simple identification of 0.25 pH changes. Images highlighted within the figure are cropped smartphone images through the fibre optic cable, images of the whole illuminated are of the hologram are demonstrated in Fig. S7. The homogeneity of colour with increasing wavelength can be seen to be consistent with minimal variation over the illuminated area. Quantitative analysis allows for more accurate determination of pH. A linear trend was observed from pH 7.25 to 8.50, with a wavelength shift of 159 nm. Translating to a shift of 106 nm per pH unit, offering an ability to distinguish fluctuations of 0.009 pH units per nanometre. The optimised concentration of DMAEA was identified to 25 mol%, with a reflection peak range of 172.7 nm.

2.5. Cross-linker density dependency

As holographic sensors swell, the fringe spacings expand, tuning the wavelength reflected (Yetisen et al., 2014d). Crosslinker density is directly related to the equilibrium swelling of the system, with higher crosslinking reducing the swelling capability of the sensor, and therefore diminishing sensitivity (Orakdogen and Celik, 2016). Optimisation of hydrogel sensors was achieved with alteration of pre-polymer solutions where crosslinking densities were set to 2 mol%, 4 mol%, and 6 mol%. To ensure comparability, the second hydrogel formulation was kept consistent. Functional co-monomer concentration and dilution were kept constant at 25 mol% and 1:1 (v/v), respectively. Variation in Bragg peak shift is illustrated in Fig. 5d–f. Comparing the shifting range of 2 mol% at 227 nm (Figs. 5d) and 6% at 89 nm (Fig. S8), the relationship is clearly established between crosslinker density and shifting range. Decreased crosslinker density of sensors allows for a greater expansion ranging from the high UV to the low IR (Fig. 5e). At 6 mol% of EGDMA, considerable shifting of the Bragg wavelength is still observed, but response is muted in comparison. 2 mol% of crosslinker density displayed the largest Bragg peak shift, with a linear relationship from 691 nm at pH 7.25–471 nm at pH 8.75, translating to a sensitivity of 146 nm/pH unit (0.0068 pH nm^{-1}) (Fig. 5f). However, consistency of the wavelength observed was diminished, reducing readout reliability. As EGDMA concentration is reduced, the peak equilibration range increases. 4 mol% of EGDMA was selected as the ideal crosslinking density, offering adequate shifting range from the red region at pH 7 (648 nm) to the blue region at pH 9 (475 nm) whilst maintaining reliability. Herein, hydrogels were demonstrated to show optimum responses with whole spectrum shifting range and fast response time, when the responsive matrix was fabricated with a 25 mol% of DMAEA, 4 mol% of EDGMA crosslinker and a hydrogel thickness of 30 μm.

Optimised hydrogel sensors were applied to holographic recordings of more complex images utilising mirrored templates structures to convey further information to the user. This is achieved *via* the use of a mirrored stencil on a non-reflective background to record shapes or letters (Fig. 5g). The recording of the additional information for the user can improve the clarity of results to viewers and minimises the risk of confusion when analysing *via* the spectrophotometer. Fig. 5h highlights the response of artistic holograms, when analyte pH is varied from 7 to 9. A homogenous color change across the lettering was observed, indicating the variation of conditions within the analyte, with the lettering recorded highlighting the stimuli the sensor is responsive to pH (Movie S2). The recording of text opens the opportunity for POC applications, an example may be in the form of a plaster-based device that can identify the change in physiological conditions and indicate the stimuli without the requirement for any additional equipment. This vital information can better inform care providers of some of the initial warning signs to assign treatment faster and reduce the severity of the ailment.

Supplementary data related to this article can be found at https://doi.org/10.1016/j.bios.2022.114206.

2.6. Application of holographic hydrogel pH sensor

Holographic sensor reliability and selectivity in the presence of common biological contaminates was determined *via* the variation of pH from 7.4 to 9.0 in a variety of analyte solutions (Fig. 6a). Independence of the salt utilised was confirmed by maintaining ionic strength with NaCl in replacement of KCl. A negligible variation of 10 nm in total shift was observed. To test the possible interference of physiological concentrations of carbohydrates and proteins, glucose (100 mmol L^{-1}) and albumin (3.94 g/L) were added to TRIS buffers, at pH 7.4 and 9.0. The results clearly show a similar relationship for both samples to the blank KCl buffer with minimal effect on the replay wavelength. The holographic sensing platform developed clearly exhibits selectivity to solution pH without interference by common biological contaminates, due to the absence of functional groups capable of binding or interacting with contaminate analytes. Sensor resilience against interference is linked to the composition of the polymer, both HEMA and EGDMA are unable to generate a fixed ionic charge within the hydrogel, therefore being unable to initiate the required volumetric change within the sensor. The tertiary amine group of DMAEA reduces the probability of irreversible covalent or substitution reactions occurring with contaminates within the sensor due to the strength of the C–N bond. Although theoretically the lone pair of electrons would be able to interact with the positively charged ionic species, the affinity of this binding is expected to be below the threshold to facilitate binding and swelling. The absence of interaction can be observed in the minimal effect of changing the ionic species between K^+ and Na^+.

Reliability and reversibility of the holographic pH sensors are imperative in their application to continuous monitoring of metabolites. To demonstrate the high reversibility and applicability of sensors to continuous measurement, holographic sensors were repeatedly submerged in pH 7 and 9 (TRIS, [50 mmol L^{-1}]) buffer solutions 20 times to observe variation in replay wavelength (Fig. 6b). Sensors exhibited minimal variation in the reflection wavelength when swollen at pH 7, error range of ±16 nm. At pH 9, an error range of ±7 nm is observed. It

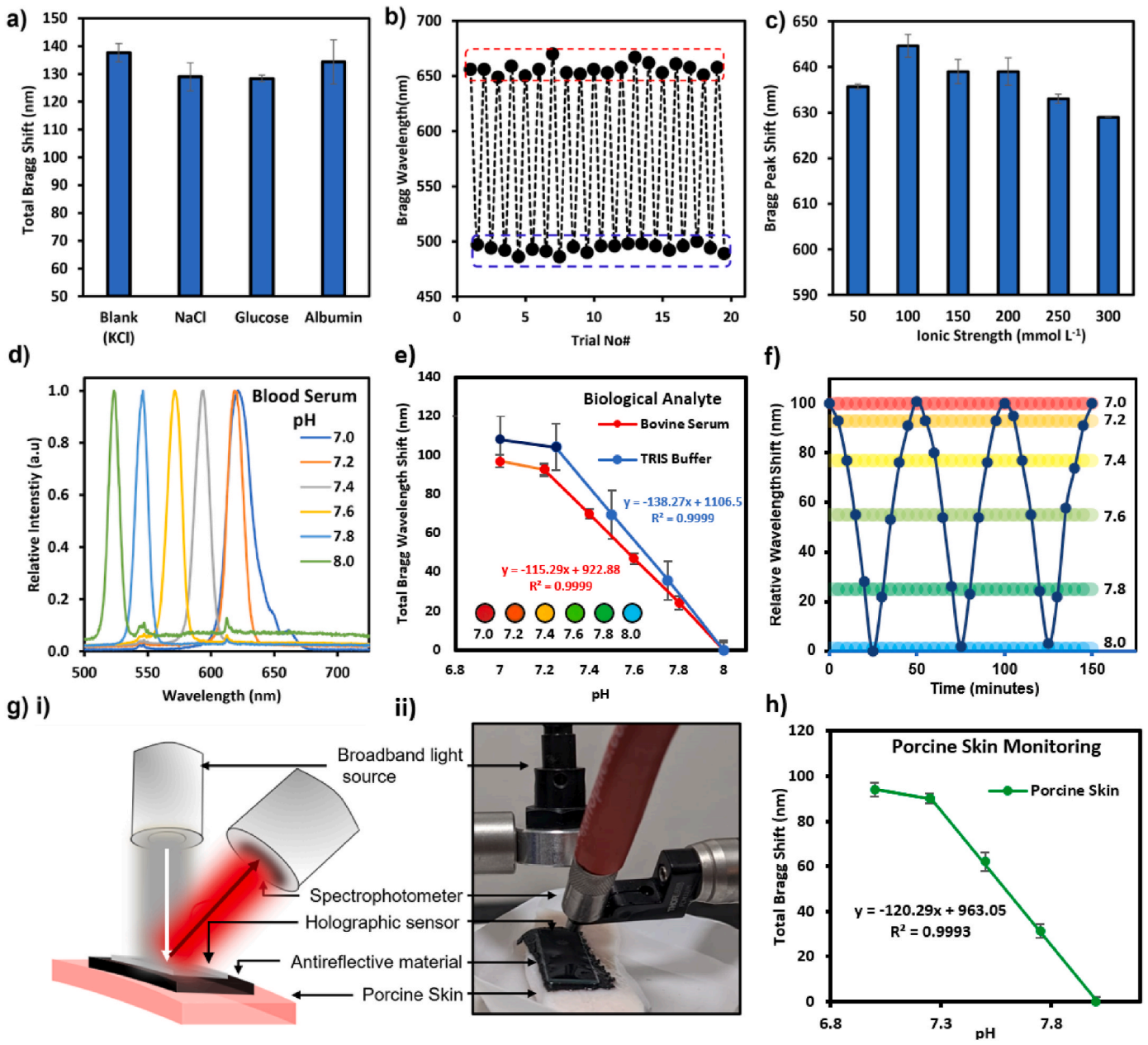

Fig. 6. Recording of patterned holographic gratings and measurements to demonstrate sensor characteristics with a composition of DMAEA (25 mol%) and EGDMA (4 mol%). a) Demonstration of the total Bragg peak shift for selectivity experiments varying pH from 7.4 to 9.0 by changing the ionic salt and contaminating buffers with common biological substances. b) Reversibility measurement cycling to demonstrate reusability of the sensor, where red and blue dashed boxes highlight the region of variation for pH 7.0 and 9.0 respectively. c) Holographic sensors were moved between solutions of constant buffer concentration whilst ionic strength was varied from 50 mmol L^{-1} to 300 mmol L^{-1}. d) Normalised Bragg reflection wavelength collected throughout the blood serum measurements, where error bars represent the standard error of. e) Calibration curves comparing spectral response in bovine serum vs buffer solutions over the range of pH 7–8, insets highlight the colour reflected at specified pH values in bovine serum, where error bars represent the standard error of 3 independent sets of results. f) Relative wavelength change of holographic sensors continuously monitoring of bovine serum pH from pH 7–8. g) Schematics highlighting the spectrophotometer setup utilised to analyse holographic sensor response in an *ex-vivo* setting. h) Total change in Bragg peak that occurs with the change of pH from 7 to 8 in *ex-vivo* model plotted against monitoring of pH in TRIS buffer solutions, where error bars represent the calculated standard error of 3 independent sets of results.

is hypothesized that due to the greater level of swelling at pH 7, more variation can arise and therefore incur minor alterations in replay wavelength. Although the change is relatively small, this is a factor that requires further attention in future works. The sensors, however, clearly demonstrate a high level of reversibility between pH measurements, allowing devices to be utilised for continuous monitoring without recalibration.

The volumetric change of holographic sensors is correlated with the generation of ionic species within the pH sensitive layer leading to the movement of ions across the hydrogels. Ionic strength interference required testing to determine the sensor dependency (Brannon-Peppas and Peppas, 1991; Bajpai et al., 2008). Ionic strength of buffers can be affected by variations in the ionisation of functional groups and the presence of salts within solutions. In previous monomer variation experiments, to ensure pH was the stimulus of swelling behaviour, buffer concentrations remained constant and ionic strength was corrected *via* addition of a mono ionic salt (KCl). To demonstrate that the replay wavelength is independent of ionic strength, a holographic sensor was

submerged in a range of test solutions where the buffer concentration is maintained at 50 mmol L^{-1} and ionic strength is increased from 50 to 300 mmol L^{-1} (Fig. 6c). There was observable variation upon initial changing of solution, hypothesized to be linked to sensor equilibration from increases or decreases in ionic strength. However, it can be assumed that the influence of ionic strength over the physiological range is minimal, with a variation of 14 nm from maxima to minima.

To further demonstrate the opportunities and potential applications, the developed holographic sensors were used to analyse the pH of bovine serum samples (Fig. 6d). To adequately stabilise pH of the analytes a high molarity TRIS buffer (1 mol L^{-1}) was utilised over a range of 7–8, increasing in increments of 0.2 pH units. Calibration curves comparing biological analyte response against response observed in a TRIS buffer (50 mmol L^{-1}) (Fig. 6e), insets demonstrate the reflected colour observed from a fibre optic cable, with a linear relationship for pH values from 7.2 to 8 permitting quantitative colourimetric pH identification over this range. A similar trend in results is observed with the replay wavelength plateauing below pH 7.2 and decreasing in a linear trend as pH is increased, validating the applicability of the developed devices to application in biological analytes. The minimally diminished response in serum when compared to the buffer system, it is hypothesized to be linked to the significantly higher ionic strength (estimated ~0.15 mmol L^{-1}) and high number of contaminates such as multivalent ionic species present within serum interfering with the hologram response minimally. To achieve a viable continuous monitoring device, replay wavelength consistency over several cycles is vital. To highlight the reproducibility of results, sensors were cycled from pH 7–8 in bovine serum to mimic a biological system (Fig. 6f). The sensors deliver a viable continuous response in serum with minimal hysteresis in the response, and clear colour changes between each incremental pH change. To demonstrate the holographic sensors viability as a point-of-care testing device, the holographic sensor was tested on an *ex-vivo* porcine skin model (Fig. 6g). The holographic sensor was placed hydrogel facing downwards onto an absorbent antireflective polyester material and TRIS buffer solutions (pH 7–8) were pipetted on to the polyester material, washing three times prior to obtaining a measurement. The antireflective coating was utilised to minimise interference from specular reflection from the skin surface. Holographic sensors have been demonstrated viability in a real point of care analysis technique comparable to the use of a plaster or sweat sensing application. The wavelength shifting observed is highlighted in Fig. 6h, where no hysteresis is shown between prior experimental results and *ex-vivo* monitoring. Sensors thus far have demonstrated a continuous monitoring viablity with biological analytes, minimal sample volumes (100 μL), and in *ex-vivo* analysis. These characteristics are hoped to provide a sensing platform with viability towards POC wound monitoring analysis through the use of smart plasters. A requirement for incorporation of the smart material into a plaster could be achieved through the minimisation of sensor in the recording step and the building of a smartphone app to facilitate continous wound angiogenisis monitoring to improve medical care.

3. Conclusions

A single flash UV photo-polymerized fabrication technique has been utilised to produce NP-free holographic hydrogel pH sensors. This approach removes a barrier which hindered the application of holographic sensors in implantable devices (Asare et al., 2012). Functionalised dual photopolymerised sensors show high sensitivity and selectivity in biological fluids. Variation of nanoscale fringe crosslinking density within a smart pH responsive hydrogel material facilitates the tuning of reflection wavelength. Computational modelling of hydrogel swelling studied the effect on sensor response. Holographic sensors developed are capable of quantitatively monitoring a pH range of 7–9 *via* simple spectrophotometer analysis (Yetisen et al., 2014e). Qualitative measurements of 0.25 pH units are clearly discerned by the naked eye, reducing the equipment requirement. Ideal hydrogel thickness for response time and relative brightness (30 μm, 5 min) was determined. Sensitivity compares to conventional electrochemical sensors with the maximum sensitivity of 0.0068 pH nm^{-1}. Sensor selectivity, reliability, and independence from biological contaminate have been demonstrated. In future research, response time could be improved by increasing the porosity of the responsive matrix to enhance the diffusion across the hydrogel (Dragusin et al., 2012). Sensor miniaturization and readout optimsation through exposure optimisation would facilitate application into POC devices such as sensitive plasters and contact lenses. Sensor pK_a has been tuned for the application to specific biological analytes ranging from 7 to 9. Investigation of the effect of functionalisation with co-monomers of different reactivities could facilitate colorimetric detection of glucose, DNA or Urea (Lee et al., 2004; Naydenova et al., 2009; Kabilan et al., 2005b). Sensors have shown as viable in biological analytes, such as bovine albumin, effectively identifying pH variation.

Declaration of competing interest

The authors declare that they have no known competing financial interests or personal relationships that could have appeared to influence the work reported in this paper.

Acknowledgements

A.K.Y and Y.H. thank the Engineering and Physical Sciences Research Council (EP/T013567/1). N. J. acknowledges National Natural Science Foundation of China (No. 82102182) and the Fundamental Research Funds for the Central Universities (No. YJ202152). The authors would like to specifically thank Rebecca Clancy, Shaviaz Iqbal, and Xingchen Dong for their effort in development of this research.

Appendix A. Supplementary data

Supplementary data to this article can be found online at https://doi.org/10.1016/j.bios.2022.114206.

References

Alibrandi, G., Coppolino, S., Micali, N., Villari, A., 2001. J. Pharm. Sci. 90 (3), 270–274.
Altschuh, D., Oncul, S., Demchenko, A.P., 2006. J. Mol. Recogn. 19 (6), 459–477.
Asare, N., Instanes, C., Sandberg, W.J., Refsnes, M., Schwarze, P., Kruszewski, M., Brunborg, G., 2012. Toxicology 291 (1), 65–72.
Askadskii, A.A., 1990. Polym. Sci. 32, 2061–2069.
Bajpai, A.K., Shukla, S.K., Bhanu, S., Kankane, S., 2008. Prog. Polym. Sci. 33, 1088–1118.
Brannon-Peppas, L., Peppas, N.A., 1991. J. Contr. Release 16, 319–329.
Chattopadhyay, K., Mazumdar, S., 2000. Biochemistry 39 (1), 263–270.
Colletti, R., Christie, D., Orenstein, S., 1995. J. Pediatr. Gastroenterol. Nutr. 21, 253–262.
Cotanda, P., Wright, D.B., Tyler, M., O'Reilly, R.K., 2013. J. Polym. Sci., Part A: Polym. Chem. 51, 3333–3338.
Davies, S., Hu, Y., Jiang, N., Blyth, J., Kaminska, M., Liu, Y., Yetisen, A.K., 2021. Adv. Funct. Mater. 2105645.
De, S.K., Aluru, N.R., Johnson, B., Crone, W.C., Beebe, D.J., Moore, J., 2002. J. Microelectromech. Syst. 11 (5), 544–555.
Dincer, C., Bruch, R., Kling, A., Dittrich, P.S., Urban, G.A., 2017. Trends Biotechnol 35 (8), 728–742.
Doney, S.C., Balch, W.M., Fabry, V.J., Feely, R.A., 2009. Oceanography 22 (4), 16–25.
DPhil, B.G., BSc, A.A.H., BSc, N.P.B., BSc, J.D., 2005. J. Wound Care 14 (2), 59–61.
Dragusin, D.-M., Van Vlierberghe, S., Dubruel, P., Dierick, M., Van Hoorebeke, L., Declercq, H.A., Cornelissen, M.M., Stancu, I.-C., 2012. Soft Matter 8 (37), 9589–9602.
Gethin, G., 2007. Wounds UK 3.
Hageman, H.J., 1985. Prog. Org. Coating 13 (2), 123–150.
Howick, J., Cals, J.W.L., Jones, C., Price, C.P., Plüddemann, A., Heneghan, C., Berger, M. Y., Buntinx, F., Hickner, J., Pace, W., Badrick, T., Van den Bruel, A., Laurence, C., van Weert, H.C., van Severen, E., Parrella, A., Thompson, M., 2014. BMJ Open 4 (8), e005611.
Hu, J., Wang, S., Wang, L., Li, F., Pingguan-Murphy, B., Lu, T.J., Xu, F., 2014. Biosens. Bioelectron. 54, 585–597.
Jiang, N., Butt, H., Montelongo, Y., Liu, F., Afewerki, S., Ying, G.L., Dai, Q., Yun, S.H., Yetisen, A.K., 2018. Adv. Funct. Mater. 28 (24), 1702715.

Jiang, N., Davies, S., Jiao, Y., Blyth, J., Butt, H., Montelongo, Y., Yetisen, A.K., 2021. ACS Sens 6, 915–924.
Jones, E.M., Cochrane, C.A., Percival, S.L., 2015a. Adv. Wound Care 4 (7), 431–439.
Jones, E.M., Cochrane, C.A., Percival, S.L., 2015b. Adv. Wound Care 4 (7), 431–439.
Kabilan, S., Marshall, A.J., Sartain, F.K., Lee, M.-C., Hussain, A., Yang, X., Blyth, J., Karangu, N., James, K., Zeng, J., Smith, D., Domschke, A., Lowe, C.R., 2005a. Biosens. Bioelectron. 20, 1602–1610.
Kabilan, S., Marshall, A.J., Sartain, F.K., Lee, M.C., Hussain, A., Yang, X., Blyth, J., Karangu, N., James, K., Zeng, J., Smith, D., Domschke, A., Lowe, C.R., 2005b. Biosens. Bioelectron. 20 (8), 1602–1610.
Kang, Y., Walish, J.J., Gorishnyy, T., Thomas, E.L., 2007. Nat. Mater. 6, 957–960.
Kawata, K., Osawa, M., Okabe, S., 2009. Environ. Sci. Technol. 43, 6046–6051.
Kim, J., Campbell, A.S., de Ávila, B.E.-F., Wang, J., 2019. Nat. Biotechnol. 37 (4), 389–406.
Koch, K., Hargreaves, B., Pauly, K., Chen, W., Gold, G., King, K., 2010. J. Magn. Reson. Imag. 32, 773, 773.
Kreis, D.T., 2004. Optical Foundations of Holography. In: Handbook of Holographic Interferometry, pp. 9–80.
Lee, M.-C., Kabilan, S., Hussain, A., Yang, X., Blyth, J., Lowe, C.R., 2004. Anal. Chem. 76 (19), 5748–5755.
Leite, E., Naydenova, I., Mintova, S., Leclercq, L., Toal, V., 2010. Appl. Opt. 49 (19), 3652.
Li, Y., Wang, Z., Wei, Q., Luo, M., Huang, G., Sumer, B.D., Gao, J., 2016. Polym. Chem. 7, 5949–5956.
Luppa, P.B., Müller, C., Schlichtiger, A., Schlebusch, H., 2011. TrAC Trends Anal. Chem. 30 (6), 887–898.
Marshall, A.J., Blyth, J., Davidson, C.A.B., Lowe, C.R., 2003. Anal. Chem. 75, 4423–4431.
Marshall, A.J., Young, D.S., Kabilan, S., Hussain, A., Blyth, J., Lowe, C.R., 2004. Anal. Chim. Acta 527, 13–20.
Mayes, A.G., Blyth, J., Millington, R.B., Lowe, C.R., 2002. Anal. Chem. 74, 3649–3657.
Naydenova, I.G., Martin, S., Toal, V., 2009. Photopolymers: beyond the Standard Approach to Photosensitisation.
Ofridam, F., Tarhini, M., Lebaz, N., Gagnière, É., Mangin, D., Elaissari, A., 2021. Polym. Adv. Technol. 32, 1455–1484.
Orakdogen, N., Celik, T., 2016. J. Polym. Res. 23, 57.
Percival, S.L., McCarty, S., Hunt, J.A., Woods, E.J., 2014. Wound Repair Regen 22 (2), 174–186.
Petelska, A.D., Figaszewski, Z.A., 2000. Biophys. J. 78 (2), 812–817.
Sajid, M., Kawde, A.-N., Daud, M., 2015. J. Saudi Chem. Soc. 19, 689–705.
Shaw, J.L.V., 2016. Pract. Lab. Med. 4, 22–29.
Skou, J.C., 1998. Angew. Chem. Int. Ed. 37 (17), 2320–2328.
Smith, J.L., Doran, J.W., 1997. Methods for Assessing Soil Quality, pp. 169–185.
Song, L., Hennink, E.J., Young, I.T., Tanke, H.J., 1995. Biophys. J. 68, 2588–2600.
Tang, H., Zhao, W., Yu, J., Li, Y., Zhao, C., 2018. Molecules 24, 4.
Tjandra, A.D., Chang, J.Y.H., Ladame, S., Chandrawati, R., 2020b. Chapter 1.2 - Optical sensors. In: Ladame, S., Chang, J.Y.H. (Eds.), Bioengineering Innovative Solutions for Cancer. Academic Press, pp. 23–45.
Weidgans, B.M., Krause, C., Klimant, I., Wolfbeis, O.S., 2004. Analyst 129, 645–650.
Yager, P., Domingo, G.J., Gerdes, J., 2008. Annu. Rev. Biomed. Eng. 10.
Yetisen, A.K., Akram, M.S., Lowe, C.R., 2013. Lab Chip 13 (12), 2210–2251.
Yetisen, A.K., Qasim, M.M., Nosheen, S., Wilkinson, T.D., Lowe, C.R., 2014a. J. Mater. Chem. C 2, 3569–3576.
Yetisen, A.K., Butt, H., da Cruz Vasconcellos, F., Montelongo, Y., Davidson, C.A.B., Blyth, J., Chan, L., Carmody, J.B., Vignolini, S., Steiner, U., Baumberg, J.J., Wilkinson, T.D., Lowe, C.R., 2014b. Adv. Opt. Mater. 2 (3), 250–254.
Yetisen, A.K., Montelongo, Y., Farandos, N.M., Naydenova, I., Lowe, C.R., Yun, S.H., 2014c. Appl. Phys. Lett. 105 (26), 261106.
Yetisen, A.K., Naydenova, I., Da Cruz Vasconcellos, F., Blyth, J., Lowe, C.R., 2014d. Chem. Rev. 114 (20), 10654–10696.
Yetisen, A.K., Martinez-Hurtado, J.L., Garcia-Melendrez, A., da Cruz Vasconcellos, F., Lowe, C.R., 2014e. Sensor. Actuator. B Chem. 196, 156–160.
Zarei, M., 2017. TrAC Trends Anal. Chem. 91, 26–41.
Zulkarnay, Z., Shazwani, S., Ibrahim, B., Jurimah, A.J., Ruzairi, A.R., Zaridah, S., 2015. In: 2015 2nd International Conference on Biomedical Engineering (ICoBE), pp. 1–6.